IOP Publishing | Royal Swedish Academy of Sciences Physica Scripta

Phys. Scr. **T171** (2020) 014042 (11pp) https://doi.org/10.1088/1402-4896/ab4d72

# Metallography and mechanical parameters of plasma-exposed plasma-facing materials and components

**G Pintsuk[1], S Brezinsek[1], J W Coenen[1], A Huber[1], M Rubel[2], A Widdowson[3] and JET Contributors[4]**

[1] Forschungszentrum Jülich GmbH, Institut für Energie- und Klimaforschung—Plasmaphysik, Partner of the Trilateral Euregio Cluster (TEC), 52425 Jülich, Germany
[2] Department of Fusion Plasma Physics, Royal Institute of Technology (KTH), 10044, Stockholm, Sweden
[3] Culham Centre for Fusion Energy, Culham Science Centre, Oxfordshire, OX13 3DB, United Kingdom

E-mail: g.pintsuk@fz-juelich.de

Received 28 August 2019, revised 27 September 2019
Accepted for publication 14 October 2019
Published 6 March 2020

**Abstract**

The performance of materials in a fusion environment is strongly dependent on the loading history, potentially leading to material modification due to thermal and particle (charged and neutral) loads. One clear indication of material modification by thermal loads is the modification of the microstructure by recrystallization, which is assessed by metallographic means as well as hardness measurements. Thereby, the recrystallization behaviour of a material strongly depends on its manufacturing route, the impurity level and on plasma impact, i.e. processes related to plasma–wall interactions. In this study, surface roughness and morphology as well as metallographic examinations and investigation by indentation techniques of components coming from different joint European torus (JET) experimental campaigns were performed for the first time on tritium-containing and therefore radioactive materials and components. This comprises on the one hand standard, marker and dedicated melt tungsten lamellae obtained from the divertor. On the other hand, beryllium components covered by nickel/beryllium marker coatings from the inner wall of JET, i.e. the inner wall guard limiter, wide poloidal limiter and dump plate were investigated. These have undergone various loading conditions and temperature excursions leading to surface modifications like material erosion, deposition and melting, and have also been assessed by scanning electron microscopy and energy-dispersive x-ray spectroscopy in view of the influence of the marker layers.

Keywords: JET ITER-like wall, metallography, beryllium, tungsten

(Some figures may appear in colour only in the online journal)

## 1. Introduction

The performance of materials in a fusion environment is strongly dependent on the loading history, potentially leading to material modification due to thermal, particle and neutron loads. The main and largest facility operating to date to study these effects is the Joint European Torus (JET) at the Culham Science Centre, UK. Since its start of operation in 1983, JET has seen several updates and among those the replacement of the plasma-facing carbon wall components by the JET ITER-like wall (ILW) consisting of beryllium (Be) limiter components for the main chamber walls and bulk tungsten (W) as well as W-coated components for the divertor region [1, 2]. Since the start of operation with this new configuration in 2011, several campaigns, namely ILW-1 (2011–2012), ILW-2 (2013–2014) and ILW-3 (2015–2016), have been performed aiming at providing essential information for the

[4] See the author list of E Joffrin *et al.* accepted for publication in Nuclear Fusion Special issue 2019, https://doi.org/10.1088/1741-4326/ab2276

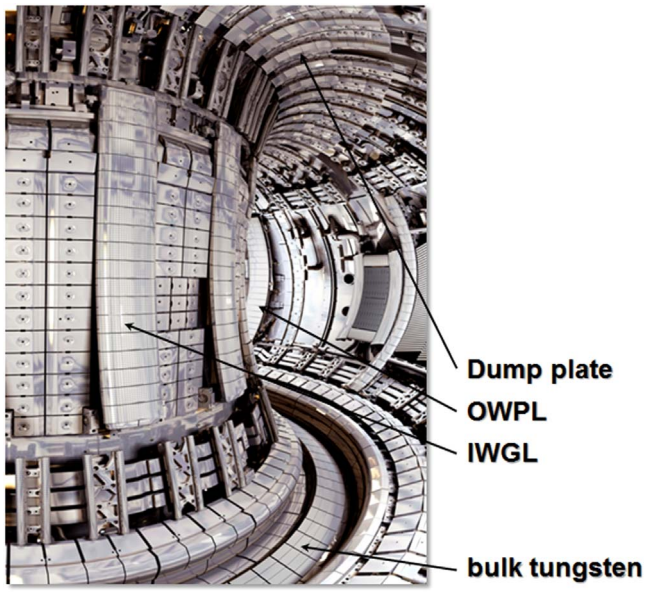


**Figure 1.** Image of the JET ITER-like wall (copyright: JET-EFDA) with indicated locations of the individually investigated components. © EFDA JET.

expected material behaviour in ITER and giving a technical basis for the development of ITER scenarios [3].

During operation, which could be in limiter or divertor configuration, thermal and particle loads were applied on these components during about 4000 discharges with a total energy input of 150.6 GJ for ILW-1, 200.5 GJ for ILW-2 [4] and 245 GJ for ILW-3. The toroidal magnetic field decays with one over the major radius (1/R) in the torus. Thus, all inner wall guard limiters (IWGL) are located on the high magnetic field side and all outer wide poloidal limiters (OWPL) on the low magnetic field side of JET (see figure 1). As the direction of the toroidal magnetic field and the plasma current is unchanged since installation of the ILW, the right- and the left-hand side of an IWGL tile can in principle be denoted as the ion- and electron-drift-side, and vice versa for OWPL tiles. Due to the complex 3D first wall structure of JET, with multiple IWGL and OWPL beams distributed in the toroidal direction and the poloidal magnetic field component during plasma operation, shadowing effects occur on these plasma-facing components, as described in more detail in [5]. These shadowing effects lead to an asymmetric distribution of particle and heat loads onto the limiters in the poloidal direction resulting in general in a stronger load on the right-hand side of the upper part and the left-hand side of the lower part of a limiter beam, as observed in discharges with limiter configuration by IR thermography and associated modelling [6]. The load is most balanced for the limiter tile positioned at the height of the plasma centre in limited magnetic configurations. The heat and particle load distribution has a vital impact on the erosion and deposition pattern on the limiters, which finally depends on the plasma conditions present in the different magnetic configurations applied in the JET experiments as described by the ERO2.0 plasma–surface interaction and transport code [5]. The extracted tiles for post-mortem analysis discussed here represent the integrated erosion and deposition behaviour.

Accordingly, the applied loads result in modifications/damage to the plasma-facing surface and also to the material itself, dependent not only on the location within the machine but also on the component geometry and the related variation in plasma exposure. The alterations of the surface and the material address mainly material erosion and deposition assessed by the use of marker coatings on selected tiles [4, 7, 8] as well as fuel retention [9, 10], both influencing the material composition and morphology [11].

In this study, surface roughness and morphology as well as metallographic examinations and investigation by indentation techniques of components coming from different JET campaigns were performed in the high-temperature materials laboratory (HML) of IEK-4, Forschungszentrum Jülich, on tritium-containing and therefore radioactive materials and components. The components analysed are comprised on the one hand of standard and marker-coated W lamellae from the divertor which have also been investigated by different means in [4] and [7]. The issue with marker coatings on bulk W lamellae has to be taken into account in analyses, as pointed out in [4]. On the other hand, Be components covered by nickel (Ni)/Be marker coatings from the inner wall of JET, i.e. IWGL, OWPL and dump plate, were investigated (see figure 1). These investigations aim at complementing the previously obtained experimental results.

## 2. Components and characterization

### 2.1. Be components

The investigated Be components were retrieved from JET after the campaigns ILW-1 and ILW-2 and comprise for both campaigns the IWGL 2XR10, the OWPL 4D14 and the dump plate 2BC2. The individual specimens were selected representing different areas of the erosion and deposition regions as shown in figure 2.

On the plasma-facing surface of all these components marker coatings [12, 13] consisting of thin magnetron sputtered 2 $\mu$m Ni and $\sim$8 $\mu$m Be layers were applied to investigate plasma-induced material erosion (see figure 3).

The loading conditions for the different Be components is quite complex with particular footprints of the plasma on the inner and outer leg depending on the attachment of the plasma during limiter operation, taking into account that damage is caused only during limiter operation [14].

### 2.2. W components

The full W outer divertor at JET is made of four stacks A–D, with A being located closest to the high field side. Each stack consists of a number of individually shaped lamellae [15]. As operation at JET and more particular the outer strike point location is usually to the low field side, i.e. stack C and D (see figure 4), stack A was used to expose specially shaped lamellae used to study the melting of W.

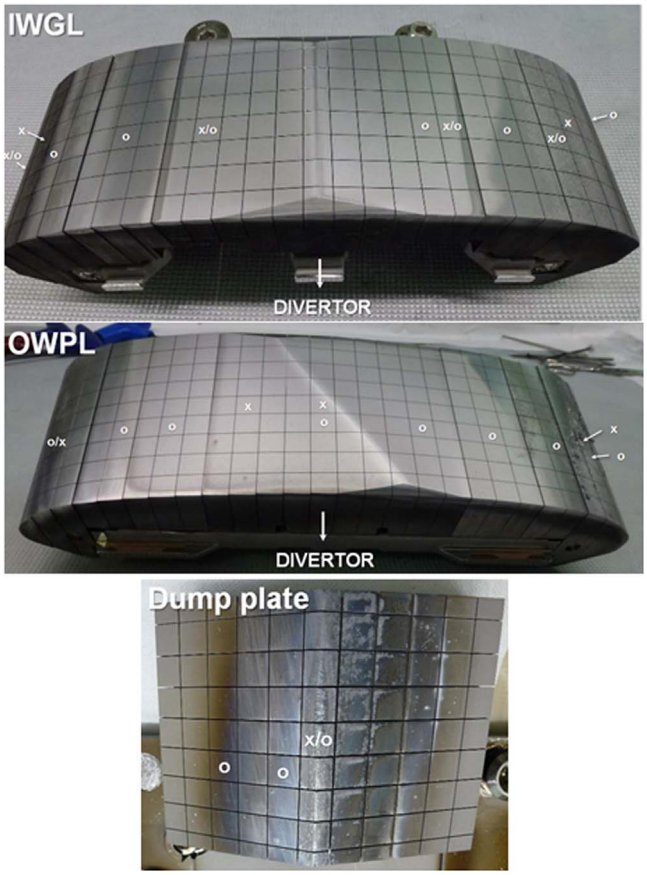


**Figure 2.** Investigated Be specimens from IWGL, OWPL and dump plate from ILW-1 (x) and ILW-2 (o).

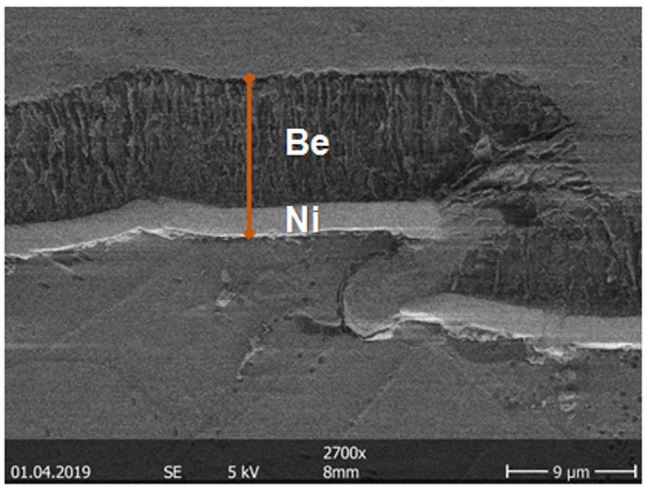


**Figure 3.** Marker coating consisting of Ni and Be.

The investigated components were taken on the one hand from ILW-1 and consist of specimens cut from a single standard lamella on stack A and standard and marker-coated lamellae positioned on stack C (see figure 5), all originating from the bulk W tile 5. The location and dimension of the investigated specimens are shown in figure 6 representatively for lamella C23. Here, the marker coating [16, 17] consists of 6 $\mu$m Mo and 6 $\mu$m W applied on the surface of bulk W (see figure 7).

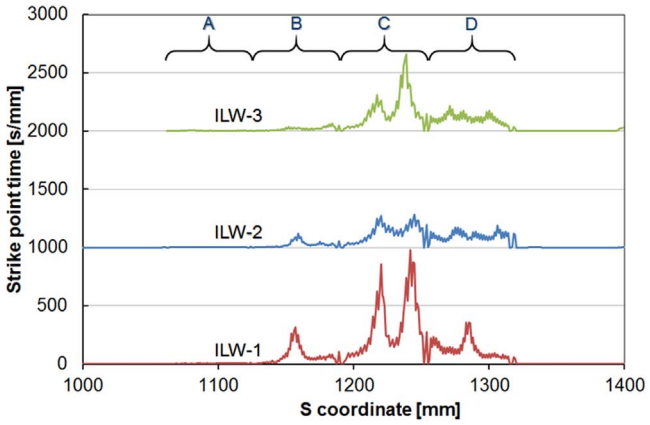


**Figure 4.** Strike point location on the full W divertor during ILW-1 to 3; S-coordinate provides the location in the divertor schematically shown in [11].

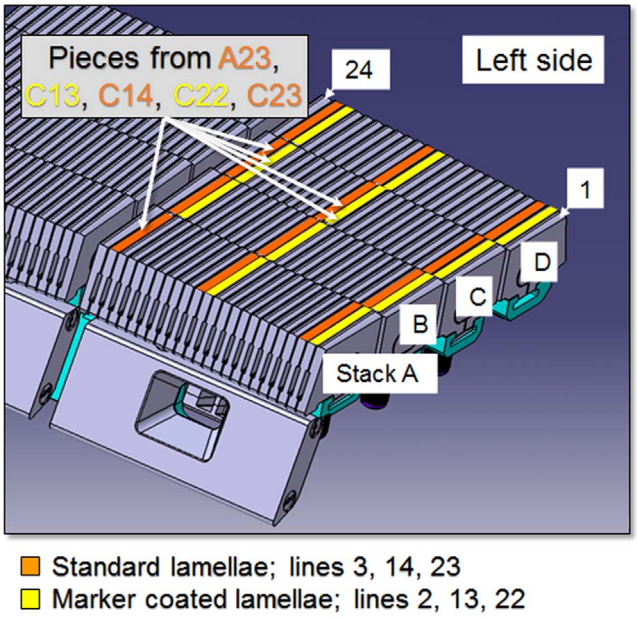


**Figure 5.** Location of investigated lamellae from ILW-1.

On the other hand, the W lamella A14, used for dedicated W melt studies, from ILW-3 was retrieved and analysed. The modified lamellae provided a protruding edge along part of the surface by introducing a raised and sloped surface. The increased surface inclination enabled easier observation of the temperature rise via IR camera and determination of the parallel heat flux [18, 19].

A macroscopic image of the lamella stack in JET is shown in figure 8, where the standard part of the lamella in the following is called part A and the inclined part of the lamella with a length of 20 mm is called part B.

The standard operational conditions in the divertor representing 90% of the performed discharges are a heat load of 60 MJ per stack integrated also over the applied edge localized modes (ELMs) resulting in a surface temperature of $\sim$1200 °C measured by IR camera. Thereby, the ELMs cause a surface temperature increase of 50–200 °C for about 1 ms

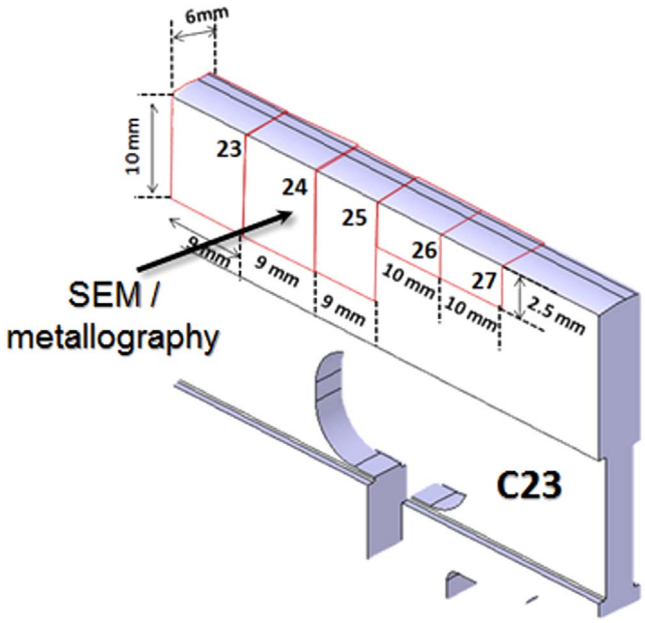


**Figure 6.** Location and size of investigated specimens for SEM and metallography for the standard lamella C23.

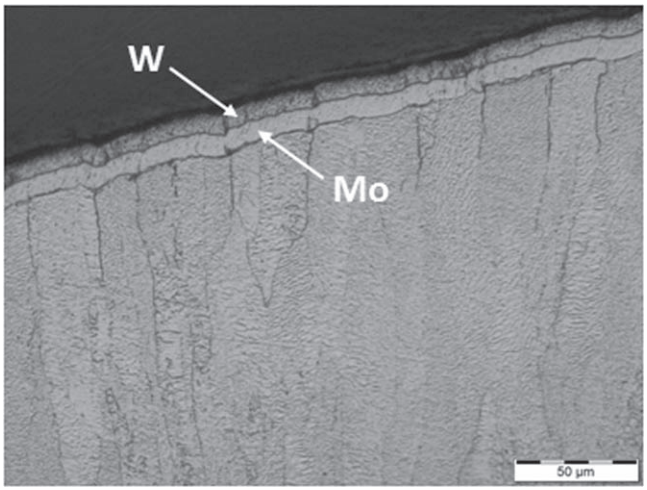


**Figure 7.** 6 $\mu$m W/6 $\mu$m Mo marker coating on top of bulk W.

per ELM with a heat penetration depth in W of ~400 $\mu$m and with 1–2 $\times$ $10^5$ ELMs per campaign. In addition, discharges up to 1700 °C were performed as well as 20–30 discharges with a total duration of ~100 s leading to surface temperature increases up to 2000 °C on stack A and B, which were used to cause melting on the special lamellae.

### *2.3. Characterization techniques*

The investigations of the individual specimens were done consecutively by the following means:

- Determination of the surface roughness by laser profilometry (OPM laser profilometer with a confocal sensor) with a measurement speed of 10 mm $s^{-1}$ and a measurement frequency of 1 kHz. The maximum accessible height difference is 1 mm and the precision of the profile is 0.02 $\mu$m.

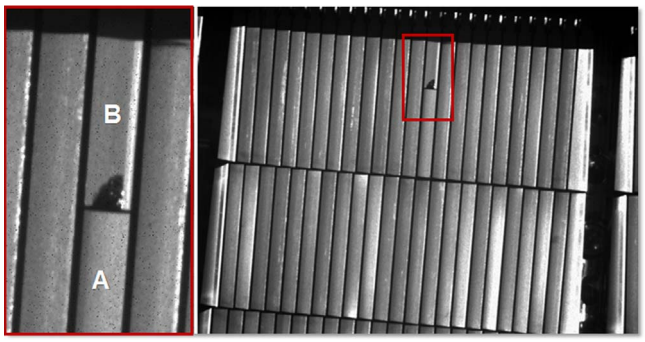


**Figure 8.** Macroscopic image of the melt lamella A14 (ILW-3) in JET [19].

- Investigation of the surface morphology and composition by a ZEISS Gemini scanning electron microscope (SEM) and an energy-dispersive x-ray (EDX) detector from Oxford Instruments.
- Metallographic investigation of material cross-sections prepared on cut and embedded specimens by grinding, polishing and etching.
- Hardness measurements on the surface of the metallographic cross-section were performed with an MHT-10 Vickers indenter from the company Anton Paar with a range for the applicable force from 0.005–4 N. The used parameters for Be and W were 0.5 and 1 N, respectively.

## 3. Results and discussion

### *3.1. Be components*

The surface roughness values determined for the different regions of the IWGL, OWPL and dump plate are shown in figure 11 by comparing, where available, identical positions on the components for ILW-1 and ILW-2. Thereby, the determined surface roughness Ra for the erosion zones of IWGL and OWPL is rather homogeneous and comparably low in the range of 1 $\mu$m for the OWPL and 1–2 $\mu$m for the IWGL, independent of the campaign.

Surface images from the erosion zones, exemplarily shown in figure 9, in combination with metallographic examination show that for the OWPL, the full marker layer has been eroded and that the interaction with the plasma has created directionally oriented erosion patterns. For the IWGL parts of the marker layer, in particular some very shallow remains of the Ni interlayer, varying in amount depending on the location, are still visible on the surface. This explains why, in contrast to the OWPL, there is still some variation in surface roughness for the IWGL.

For deposition zones on either end of the OWPL an increase in surface roughness was found from ILW-1 to ILW-2, which is very strong on the right-hand side. In contrast, hardly any variation was observed between IWL-1 and IWL-2 for the IWGL. For the IWGL one part of the explanation is that for both campaigns surface melting occurred as shown in figure 10.

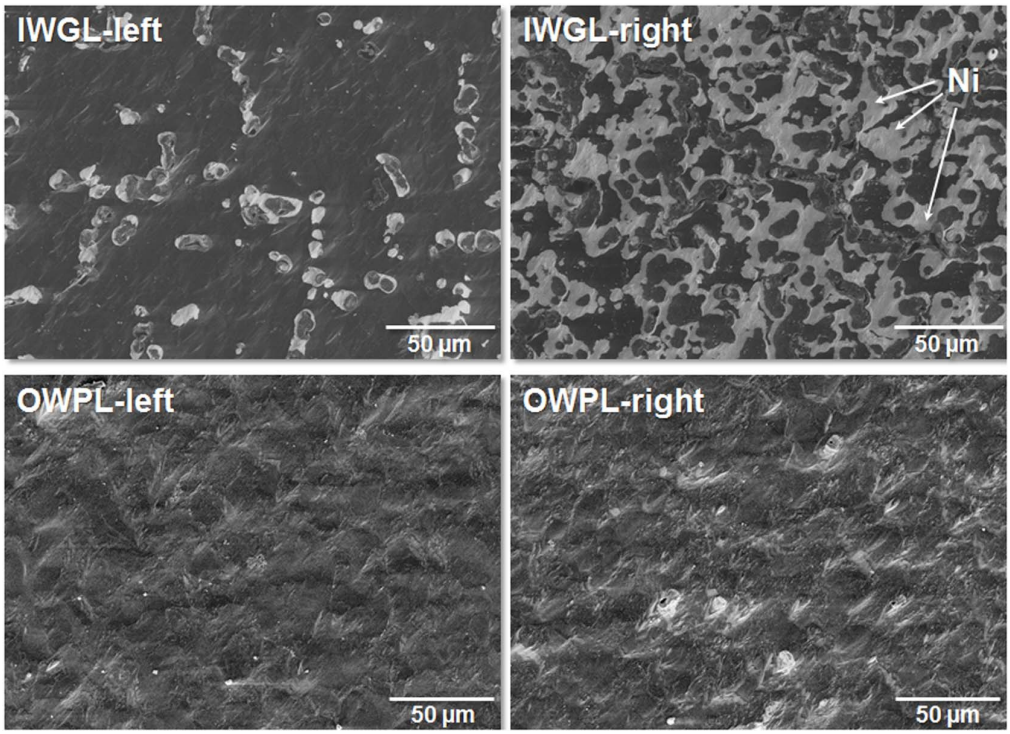


**Figure 9.** SEM images of the IWGL and OWPL surface at different locations of the erosion zone for ILW-2.

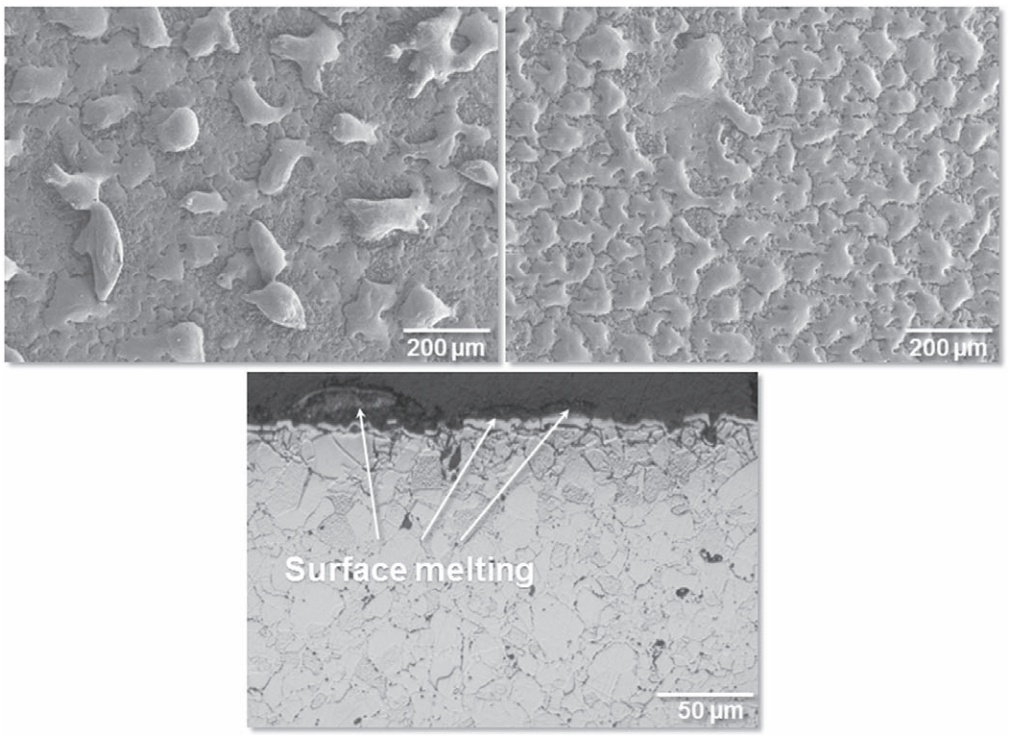


**Figure 10.** SEM images and metallographic cross-section of a specimen taken from the centre of the deposition zone on the right-hand side of the IWGL (ILW-1).

The second part of the explanation is that from the cross-sectional observation the melting can relate to just the Be layer of the marker coating or the full Be/Ni marker coating depending on the location on the component, i.e. increasing damage following the curvature of the surface and getting closer to the edge of the component. An accompanying factor is that due to melting the amount of deposition cannot be determined. However, based on thickness measurements of

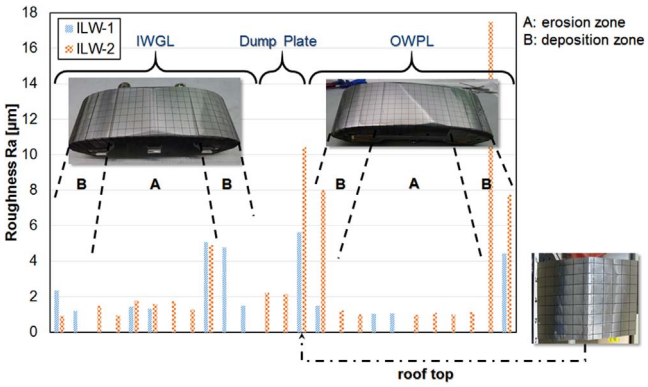


**Figure 11.** Surface roughness of Be specimens from IWGL, OWPL and dump plate—ILW-1 versus ILW-2.

the molten layer it is assumed that low or even no additional material deposition has taken place, at least for the investigated specimens and locations.

For the OWPL the dominating damaging mechanism on the right-hand side is delamination and subsequent ablation of solid material, which causes in the case of delaminated but not fully ablated material an increased surface roughness (see figure 12, ILW-2). In addition and in contrast to ILW-1, cross-sectional analyses for ILW-2 showed that material deposition on top of the marker coating has taken place consisting of Be, Ni and some W together with oxygen and carbon, which was determined to add up to 30 $\mu$m in thickness on top of the existing marker layer, which was also found for the left-hand side where it was deposited homogeneously without any indication of delamination.

With regard to the use of the applied marker layer for the determination of Be erosion, in previous studies done by elastic backscattering and nuclear reaction analysis, neither the erosion zone due to more or less full erosion of the marker layer nor the deposition zone on the right-hand side due to melting or material delamination and ablation prove in this case to be useful. However, there is a narrow transition region from the erosion to the deposition area on both sides, where an intact marker layer shows erosion of the Be top layer only. In this narrow region the erosion is influenced by the original surface roughness or waviness of the bulk material as the result is a smoothened/flattened surface with a locally varying Be layer thickness within a few tens of $\mu$m, exemplarily shown in figure 13. How large this transition zone is could not be quantified due to the limited number of available specimens. However, this is shown to be of the order of 15 mm from ion beam analysis studies [20].

In contrast to the limiters, the dump plate at the upper part of the main chamber wall is characterized, amongst others due to its particular shape, by strong melting at the roof top and on the right-hand side. The amount of melting strongly increases from ILW-1 to ILW-2 as indicated by the depth of the molten layer from ~70 to 400 $\mu$m in the roof top region (figure 14). The strong increase in melting of the dump plate tiles during ILW-2 is associated with experiments in JET to study vertical displacement events [21]. Furthermore, profilometric line scans show that while for ILW-1 the effect is low and difficult to quantify, for ILW-2 the very peak of the roof top was flattened at a width of about 1.5 mm. This comes together with a loss of about 150–200 $\mu$m in height, which is accompanied by material migration towards the left-hand side and potentially also by material erosion.

Also shown in figure 14 is the melting-induced crack formation in the material. In contrast to the acceptance criteria for ITER [22], the cracks proceed from the molten (and solidified) area towards the parent bulk material. Thereby, the penetration depth increases from ~100 $\mu$m for ILW-1 to ~200 $\mu$m for ILW-2 most probably as a result of the increased energy input.

Finally, hardness measurements were performed on the plasma-loaded side, i.e. about 100 $\mu$m from the top surface and on the back side of the 3 or 10 mm thick specimens. Despite local inhomogeneities, the results, exemplarily given for ILW-1 in figure 15, being also representative for ILW-2, show in the tested depth ranges no material modification that might for example be caused by recrystallization or diffusion of plasma species. Tackling more surface-near effects up to only a few $\mu$m in depth would require the use of nano-indentation techniques.

### *3.2. W components*

*3.2.1. Standard and marker lamellae, ILW-1.* The W lamellae were produced using electro-discharge machining without subsequent surface treatment. As a result, the surface of the W lamellae is characterized from the beginning by a micro-crack network with a crack depth of up to ~50 $\mu$m and a roughness *Ra* of ~2 $\mu$m. Investigation of the surface as well as the cross-section of the standard lamellae A23 without any strike point exposure and C14, located in the centre of tile 5, showed that thermal loading applied during ILW-1 had no clear measurable or visible effect on the surface roughness and the micro-crack network (see figures 16 and 17).

In contrast, lamella C23 taken from the hot, i.e. highest loaded, part of the tile showed erosion and near-surface melting in particular along crack edges leading to a partial coverage of the existing crack network. The erosion and melt formation also induced a slight decrease of the surface roughness, and in addition an increase in crack depth up to ~150 $\mu$m for selected initially existing cracks (see figure 17) was observed. Irrespective of these changes, no modification of the material microstructure, in particular due to recrystallization-induced grain growth, was observed.

For the marker lamellae a similar behaviour as already observed for the Be marker layers on the OWPL was determined. For lamella C22 located at the highest loaded part of the stack the coating was completely removed and similar to C23 the maximum crack depth increased. The erosion on C13 located in the centre of stack C was dominated by material delamination and subsequent ablation or melting (see figure 18). Based on the metallographic results the mechanism for the erosion is in a first step the local delamination of the W coating, resulting in a full ablation or localized melting due to the loss of thermal contact. In a second step, the same process is found to take place for the molybdenum layer. In the investigated and

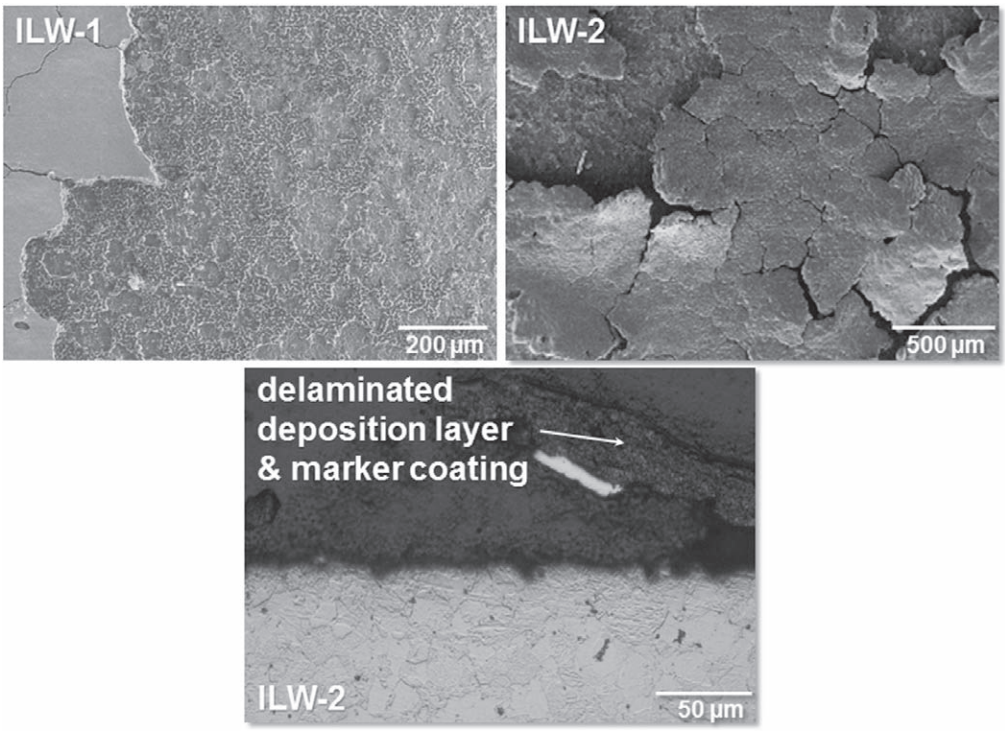


**Figure 12.** SEM images of the deposition zone on the right-hand side of the OWPL for ILW-1 and ILW-2; metallographic cross-section for the ILW-2 specimen.

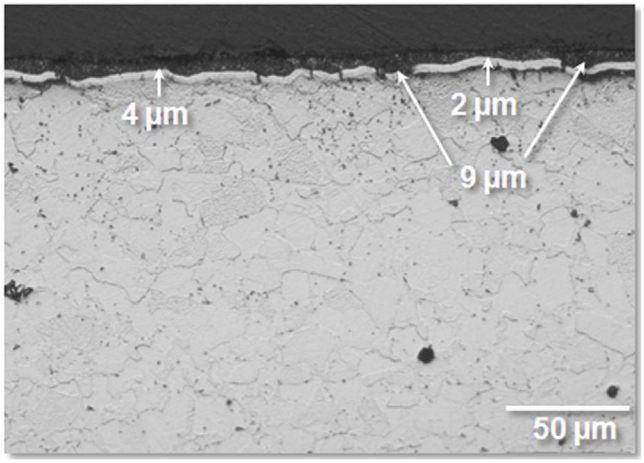


**Figure 13.** Be layer thickness in the transition zone between erosion and left-hand deposition area (ILW-2).

representatively chosen cross-section there was no clear indication of a continuous erosion of W. However, it should be noted that metallographic cross-sections provide data in limited regions and therefore it cannot be excluded that areas showing a continuous thinning of the W marker layer also exist in other regions of lamellae. This is indeed the case as ion beam analysis of these and other W lamellae from ILW-2 have shown erosion of the W marker layer of up to 1.5 $\mu$m following ILW-2 [4, 23]. However, delamination was also noted for stack D samples, making ion beam analysis (IBA) difficult.

These results indicate that the thermal loads were high enough to cause delamination of marker coatings, making it difficult to assess continuous erosion of the W coatings in the highest loaded region as well as the central part of the tile.

In contrast to the Be components, either hardening of W at the front surface or softening at the back surface was observed. As shown in figure 19, the hardness value at the surface, i.e. at a depth of $\sim$100 $\mu$m is on average higher by $\sim$25 HV1 compared to the properties at the back, i.e. at a depth of $\sim$9 mm. This might be on the one hand attributed to the material manufacturing, i.e. electro-discharge machining during manufacturing or specimen fabrication, or on the other hand to the interaction with the plasma and in particular hydrogen. In order to assess this without the option of using an as-produced non-loaded lamella, measurements of the hardness in steps of $\sim$500 $\mu$m from the front surface to the back were performed as shown in figure 20 for lamellae C14 and C23. The hardness of both lamellae is, despite the variation in microstructure between C14 and C23, identical. The same is valid for the slope of the implemented trendlines showing a slightly decreasing tendency towards the back side. In particular the value right at the back is clearly lower, which is not yet understood and does not support any of the aforementioned theories. Accordingly, this topic needs further investigation in the future.

Besides and despite the lack of recrystallization in the tested regions, in view of the normal operation conditions in the vicinity of the typical recrystallization temperature of W of $\sim$1300 °C and the limited thermal propagation distance of ELM-induced heat pulses, it would be required to tackle more surface-near effects up to only a few $\mu$m in depth by nano-indentation techniques.

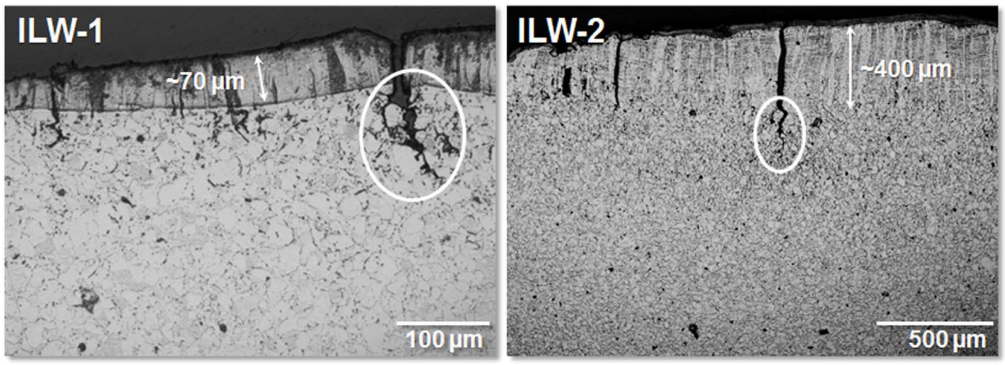


**Figure 14.** Melting and crack formation in the roof top region of the dump plate for ILW-1 and ILW-2.

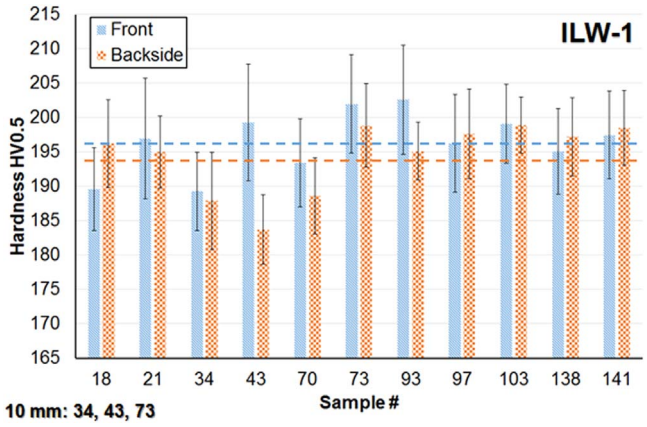


**Figure 15.** Hardness of Be specimens from ILW-1 on the front surface and the back side of the 3 and 10 mm thick specimens; IWGL (18 to 73), dump plate (93 and 97), OWPL (103 to 141) ILW-1 and ILW-2; average hardness 196.4 ± 4.4 HV0.5 (front) and 194.3 ± 5.2 HV0.5 (back).

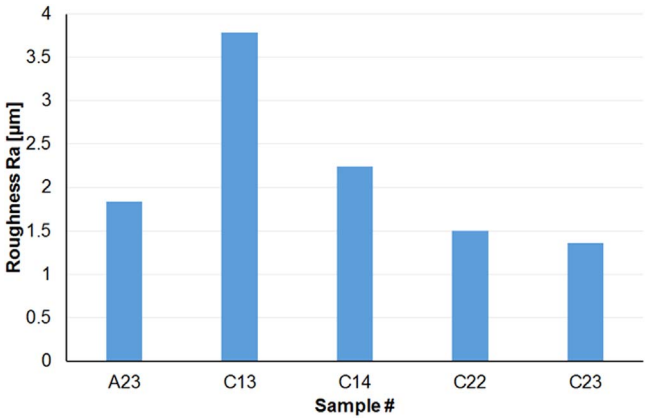


**Figure 16.** Surface roughness of the investigated lamellae.

*3.2.2. Melt lamella, ILW-3.* Strong and continuous melt formation is found in the range of ~4 mm in the poloidal direction on the sloped part B of the lamella, while small traces of melt formation are visible up to ~8 mm (see figure 21). In laser profilometry line scans the initial observation that only reduced melt motion was observed is confirmed as the surface modification is dominated by inhomogeneous material erosion (maximum depth of 100–150 $\mu$m; see figure 22).

Despite the limited area of macroscopic melt formation caused by the controlled motion of the strike point on stack A, and despite the short loading time, microscopic melt formation similar to that observed for lamella C23 from ILW-1 was also found in the inclined region up to the very edge of the lamella.

Due to the high absorbed loads on the inclined surface and the related temperature excursion, recrystallization occurred on the whole of part B of the lamella. Thereby, the recrystallization depth varied from ~5 mm in the macroscopically molten region to ~2.3 mm at the far edge (see figure 23). Related to this, the hardness of the material showing an initial average of 458 HV1, which is higher than that determined for ILW-1, decreases to an average of 395 HV1 in the recrystallized zone. For comparison, the hardness on the front surface of part A of the lamella, which does not show any surface modification, is 468 HV1, which is identical to the values determined for ILW-1. This is an indication that the hardening is most probably caused by material manufacturing and the determined values are representative for initial, non-loaded conditions of the component.

## 4. Summary and conclusions

Analyses of surface and bulk modifications of Be and W components exposed during different campaigns in JET-ILW were performed for the first time using profilometry, SEM/EDX, metallography and hardness measurements.

The results show that for the erosion zone of the Be components, the applied marker layers were fully eroded on the OWPL and heavily eroded on the IWGL with some remains of the Ni interlayer. On the high field side of the deposition zone, the damage was dominated by melting for IWGL without obvious additional material deposition and material delamination and ablation for OWPL, where an additional deposited layer of up to 30 $\mu$m was found, similar to that observed on the low field side of the components. Continuous erosion of the Be layer of the marker coating could only be clearly identified in the transition zone between the erosion and both deposition areas. The mechanical

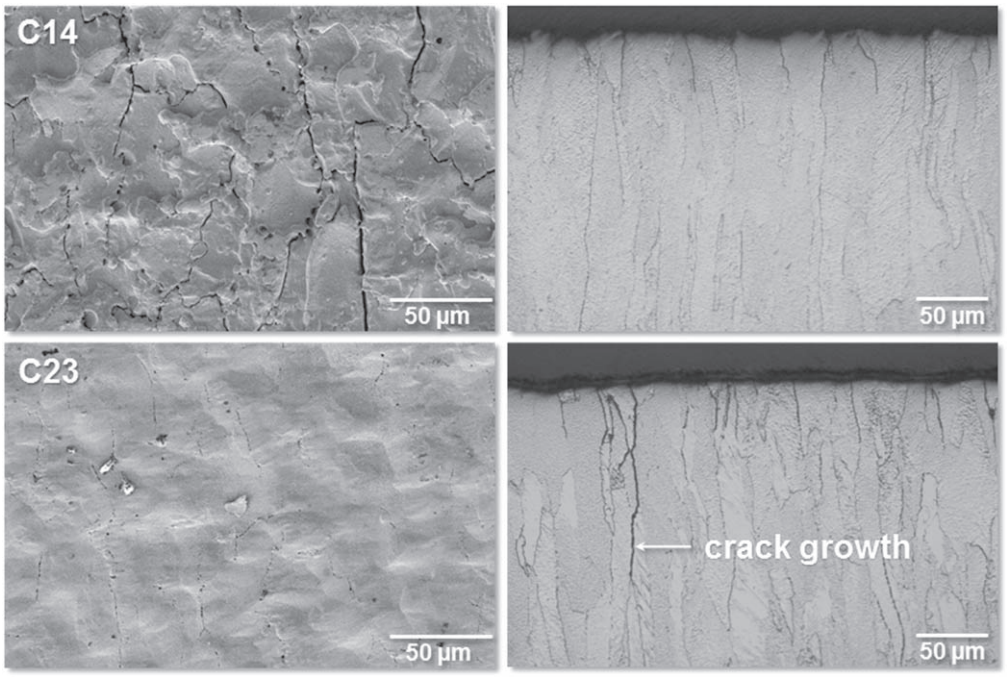


**Figure 17.** SEM images and metallographic cross-sections of the standard lamellae C14 and C23.

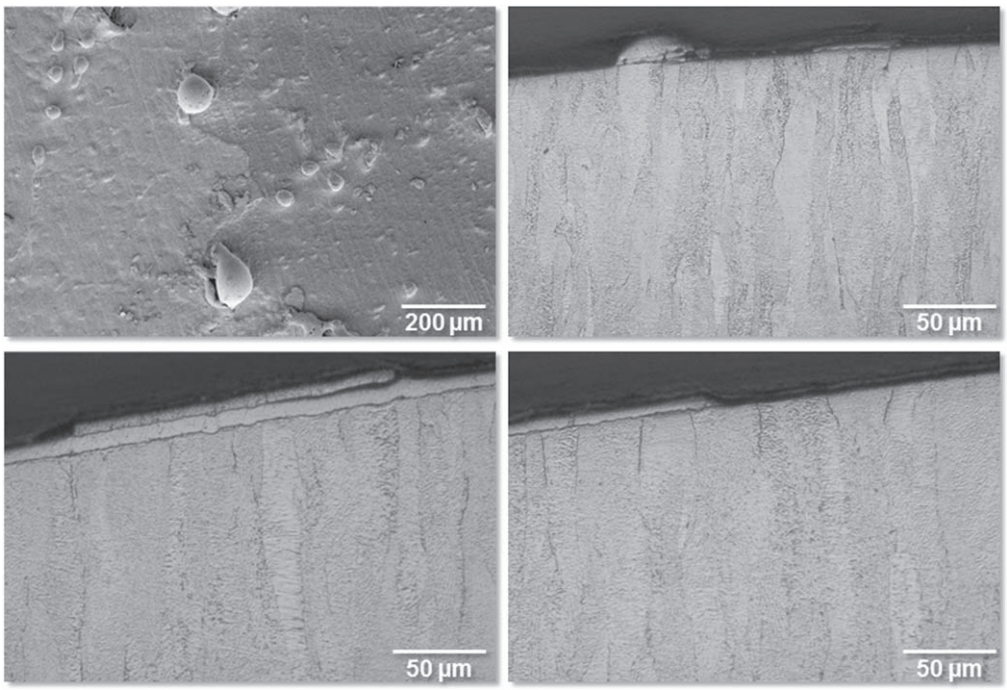


**Figure 18.** SEM image and metallographic cross-sections of the marker lamellae C13.

properties of bulk Be determined at a depth of $\geqslant 100\ \mu$m were not affected by the interaction with the plasma. A closer look at the surface-near region would require nano-indentation techniques.

For the investigated W lamellae of stack C with the highest strike point loading time, very shallow surface melting and melt motion occurred. Full erosion of the marker layer was observed on the hot side of the divertor tile, i.e. C22 and C23. In the central part, i.e. C13 and C14, no modification of the standard lamella was observed while the marker lamella was characterized by local delamination, ablation and subsequent melting of the marker layer due to the reduced thermal transfer capability. In the regions where the marker layer was still intact, no clear indication of a continuous erosion of W was found, which does not necessarily exclude its existence and indeed ion beam analysis results have been used to analyse the change in thickness of the marker coatings on the W lamellae. Similar delaminations

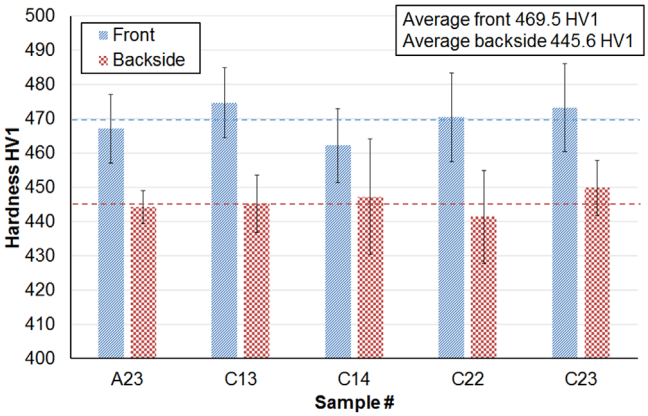


**Figure 19.** Hardness values for the lamellae of ILW-1 at the plasma-loaded front surface and on the back of the specimens.

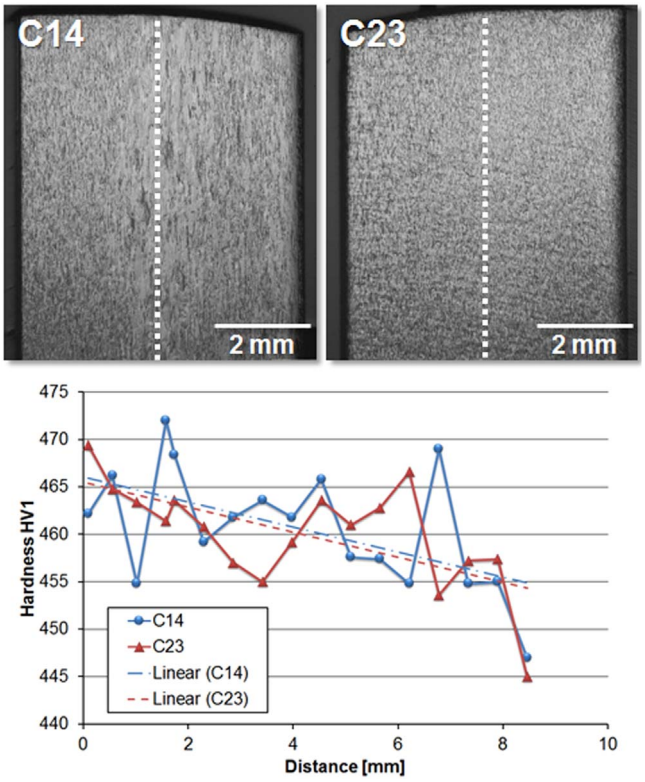


**Figure 20.** Average hardness values (five measurements each) for the lamellae C14 and C23 of ILW-1 in the centre of the lamellae from the plasma-loaded front surface to the back side of the specimens as indicated in the metallographic cross-sections.

were observed on the Be components; however, in the transition from the central part of the tile towards the shadowed region intact marker coatings have been analysed by ion beam analysis. Further evaluation of the erosion of the marker coatings on the existing lamellae by microscopy techniques would require additional analysis in other areas of the samples.

Finally, the hardness measurements yielded an increase for W in the surface-near region ($\sim$100 $\mu$m) compared to the bulk by $\sim$25 HV1 (ILW-1) and $\sim$10 HV1 (ILW-3), which


**Figure 21.** Macroscopic image of the sloped part of the melt lamella A14.

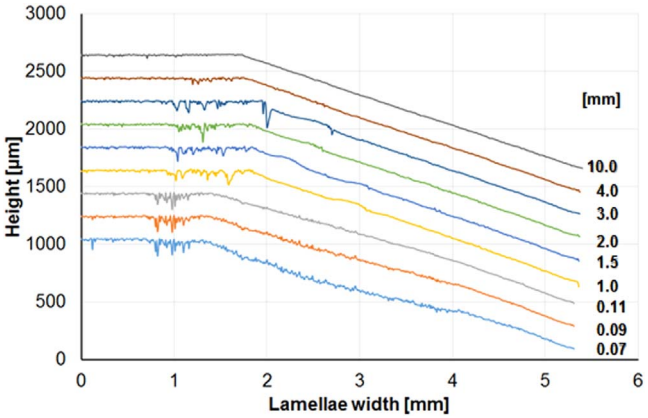


**Figure 22.** Profilometry line scans along the sloped part of the lamella from 0.07 to 10 mm in poloidal direction.

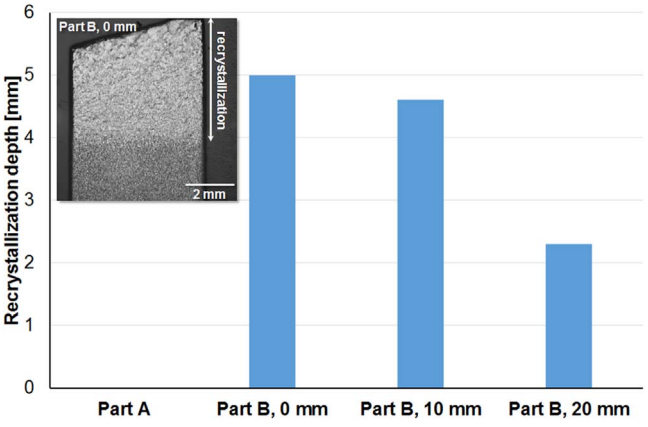


**Figure 23.** Recrystallization depth in part A and at different positions in the sloped part B of the melt lamella.

indicates that there is an influence of the plasma not in terms of temperature but by diffusion of plasma species, most probably hydrogen. This needs to be investigated further in more detail.

## Acknowledgements

This work has been carried out within the framework of the EUROfusion Consortium and has received funding from the Euratom research and training programme 2014–2018 and 2019–2020 under grant agreement No. 633053. The views and opinions expressed herein do not necessarily reflect those of the European Commission.

The work of Mrs. G Knauf, being responsible for all the experimental characterization performed within this task, is highly acknowledged.

## ORCID iDs

G Pintsuk https://orcid.org/0000-0001-5552-5427
S Brezinsek https://orcid.org/0000-0002-7213-3326
J W Coenen https://orcid.org/0000-0002-8579-908X
A Huber https://orcid.org/0000-0002-3558-8129
M Rubel https://orcid.org/0000-0001-9901-6296
A Widdowson https://orcid.org/0000-0002-6805-8853

## References

[1] Philipps V, Mertens P, Matthews G F, Maier H and JET-EFDA contributors 2010 *Fusion Eng. Des.* **85** 1581
[2] Matthews G F *et al* 2011 *Phys. Scripta* **T145** 014001
[3] Litaudon X *et al* 2017 *Nucl. Fusion* **57** 102001
[4] Mayer M *et al* 2017 *Phys. Scripta* **T170** 014058
[5] Firadouss M *et al* 2013 *J. Nucl. Mater.* **438** 536–9
[6] Romazanov J *et al* 2017 *Phys. Scripta* **T170** 014018
[7] Mayer M *et al* 2016 *Phys. Scripta* **T167** 014051
[8] Krat S, Mayer M, Bykov I, Lungu C P, de Saint Augin G, Widdowson A, Carvalho I S and JET contributors 2017 *Nucl. Mater. Energy* **11** 20
[9] Heinola K *et al* 2016 *Phys. Scripta* **T167** 014075
[10] Heinola K *et al* 2017 *Phys. Scripta* **T170** 014063
[11] Widdowson A *et al* 2017 *Nucl. Mater. Energy* **12** 499
[12] Lungu C P, Mustata I, Zaroschi V, Lungu A M, Anghel A, Chiru P, Rubel M, Coad P, Matthews G F and JET-EFDA contributors 2007 *Phys. Scripta* **T128** 157
[13] Rubel M J *et al* 2008 *J. Phys.: Conf. Ser.* **100** 062028
[14] Arnoux G *et al* 2013 *Nucl. Fusion* **53** 073016
[15] Mertens P, Coenen J W, Eich T, Huber A, Jachmich S, Nicolai A, Riccardo V and Senik K 2011 *J. Nucl. Mater.* **415** 943
[16] Maier H *et al* 2007 *Nucl. Fusion* **47** 222
[17] Rubel M *et al* 2013 *J. Nucl. Mater.* **438** S1204
[18] Iglesias D *et al* 2018 *Nucl. Fusion* **58** 106034
[19] Coenen J W *et al* 2017 *Phys. Scripta* **T170** 014013
[20] Widdowson A *et al PFMC-17 Conf. Contribution, Unpublished to Physica Scripta*
[21] Jepu I *et al* 2019 *Nucl. Fusion* **59** 086009
[22] Barabash V, Eaton R, Hira T, Kupriyanov I, Nikolaev G, Wang Z, Liu X, Roedig M and Linke J 2011 *Phys. Scripta* **T145** 014007
[23] Krat S *et al PFMC-17 Conf. Contribution, Unpublished to Physica Scripta*